

<sup>8</sup>E. C. Stoner, *Phil. Mag.* **25**, 901 (1938).

<sup>9</sup>A classical calculation of this and other hydrodynamic effects of order  $(p/p_c)^2$  has been made by C. Ebner, to be published.

<sup>10</sup>N. E. Dyumin, B. N. Esel'son, E. Ya. Rudavskii, and I. A. Serbin, *Zh. Eksp. Teor. Fiz.* **56**, 747 (1969)

[*Soviet Phys. JETP* **29**, 406 (1969)].

<sup>11</sup>W. L. McMillan, *Phys. Rev.* **182**, 299 (1969).

<sup>12</sup>G. Baym, *Phys. Rev. Lett.* **17**, 952 (1966).

<sup>13</sup>A. C. Anderson, D. O. Edwards, W. R. Roach, R. E. Sarwinski, and J. C. Wheatley, *Phys. Rev. Lett.* **17**, 367 (1966).

## MAGNETIC BUNDLES IN REACTING FLOWING PLASMA\*

V. Nardi

*Physics Department, Stevens Institute of Technology, Hoboken, New Jersey 07030*

(Received 19 June 1970)

An exact theory of plasma filaments observed in coaxial accelerators is derived from a steady-state ( $\partial/\partial t = 0$ ) description of the three-dimensional flow of deuterium plasma. Ionization and recombination reactions are considered. Magnetic structure of the filaments (bundles of helical field lines), density distributions, and flow field fit the experimental evidence.

By considering shock-wave conditions for the current sheath (CS) in coaxial accelerators (CA), it can be proved<sup>1</sup> that the plasma vorticity  $\vec{\omega} = \frac{1}{2}\nabla \times \vec{u}$  is large in the region of space where the filaments are located, immediately behind the shock front  $\Sigma$  ( $\Sigma$  is considered, essentially, as the foremost luminous face of CS). Vorticity and filament axis have the same orientation<sup>1</sup> (parallel to the  $z$  axis; see Fig. 1; without a relevant loss of generality we take  $\partial/\partial z \cong 0$ , the filaments are considered as parallel cylinders). The existence of a large  $\omega$  in a narrow region of space (containing the filaments) is not sufficient to conclude that vortex structures exist in that region. More stringently an analytic description of the plasma can be deduced which depicts the vortex nature of the filaments. The essential assumptions of the theory [see Eq. (1)] and the general results [see Eqs. (2)] are set forth below before specializing formulas to the filament problem. We can show that a strong component  $B_z$  (2500 G and larger) of the self-consistent magnetic field exists along the filament axis (orthogonal to  $B_\theta \cong B_y$ ) inside the filaments. This fact was already pointed out by magnetic probe measurements.<sup>2</sup> The density in phase space for ion and electrons  $f_\pm$  satisfies

$$df_\pm/dt = S_\pm, \quad (1)$$

where  $d/dt$  is the Vlasov operator with self-consistent fields  $\vec{E} = -\nabla\phi$ ,  $\vec{B} = \nabla \times \vec{A}$ ;  $\partial/\partial t = 0$  in the CS frame of reference (moving with a velocity  $u_0 \sim 10^7$  cm/sec in the laboratory system); the source term  $S$  accounts for ionization and recombination reactions; the indices  $\pm$  are sometimes dropped. The role of the neutral atoms is simply to affect the anisotropy in velocity of the newly born charged particles and to function as a reservoir for ions and electrons. Neutral atoms are further disregarded.  $S$  is chosen *ad hoc*, according to these criteria: (I) A solution of (1) can be obtained at a glance if a solution  $f_v$  of the Vlasov equation  $df_v/dt = 0$  is known; in our case  $f_v = f_v(\epsilon, p_z)$ , where  $\epsilon, p_z$  are ener-

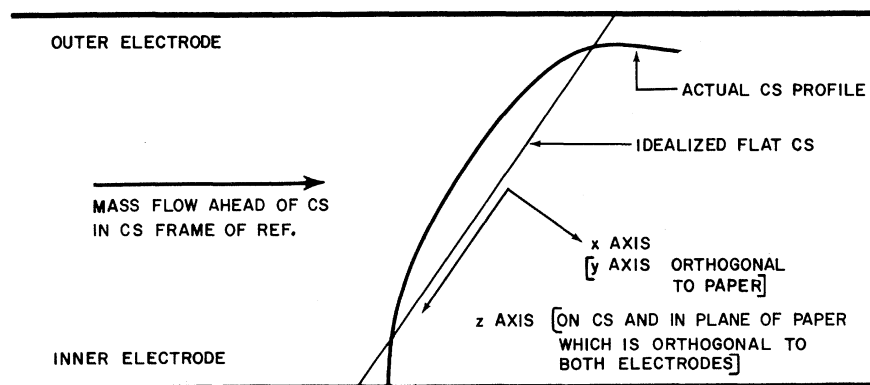


FIG. 1. Profile of the current sheath between the electrodes.

gy and  $z$  momentum of a particle; macroscopic quantities (by  $f$ ) and their relevant derivatives are continuous functions. (II) The solution  $f$  must generate specific mass and current flows [ $m_+ \rho_+ \vec{u}_+$  and  $\vec{j} = e(\rho_+ \vec{u}_+ - \rho_- \vec{u}_-)$ ] which are suggested by experimental evidence. This is conveniently accomplished by considering  $S$  as a collection of many (including a continuous distribution of) typical terms, i.e.,  $S = \sum_{i\zeta} f S_{\zeta i}$ . The particles are ejected on (by ionization) or removed from (by recombination) orbits which are defined as in the Vlasov theory and can be labeled by some constant of the motion. We chose  $\mu_{\pm}(\epsilon, p_z) = \mathcal{E}_{\pm} + \Gamma_{\pm}$  with

$$\mathcal{E}_{\pm} = [v_x^2 + v_y^2 + (v_z + c_{\pm})^2] m_{\pm} / 2, \quad \Gamma_{\pm} = \pm e(\varphi + c_{\pm} A_z),$$

$c_{\pm} = \text{const}$ ,  $c_+ > 0$ ; the typical term  $S_{\zeta i} = S_{\zeta}(\mu_i)$  then depends on a specific numerical value  $\mu_i$  of  $\mu$ . As an example, if

$$S = S_x(\mu_i) = f_v(\mu) L(\mu_i) (d/dt) [C(\psi_{xi}) C(D_{xi})],$$

where  $C(X) = 1$  if  $X > 0$ ,  $C(X) = 0$  if  $X < 0$  [the "ionization spectrum"  $L(\mu_i)$  is a constant and  $\psi_{xi} = v_x - D_{xi}^{1/2}$ ,  $D_{xi} = (\mu_i - \Gamma)(2/m) - v_y^2 - (v_z + c)^2$ ], then  $f = f_v + f_s = f_v + LC(\psi_{xi})C(D_{xi})f_v$  gives a solution of (1). For the nonlinearity of (1), the self-consistent fields in  $d/dt$ ,  $f$ ,  $S_{\zeta i}$  are always determined according to the total  $S$ . The complete theory will be presented elsewhere; we list here some of the results for the case  $f_{v\pm} = \text{const} \exp(-\alpha_{\pm} \mu_{\pm})$ ,  $\rho_{s+} = \rho_{s-}$ ,  $j_z = j_{zv} + j_{zs} = -e(\rho_{v+} c_+ - \rho_{v-} c_-) + j_{zs}$ ,  $j_{zs} = -e(\rho_{v+} c_{s+} - \rho_{v-} c_{s-})$  with  $c_{s\pm} = (c_0^2 - c_+ c_-) / c_{\mp}$ ,  $c_0 = \text{speed of light}$ ,  $u_{xs}, u_{ys} \neq 0$  (i.e., no contribution to the net charge comes from the source-controlled part  $f_s$  of  $f$ , etc.), and  $\Gamma_+, \Gamma_- > 0$ .  $A_z, \varphi$  (emu) satisfy

$$\nabla^2 A_z = 4\pi e [\rho_{0+} (c_0^2 / c_-) \exp(-\alpha_+ \Gamma_+) - \rho_{0-} (c_0^2 / c_+) \exp(-\alpha_- \Gamma_-)]$$

and a similar equation for  $\varphi$  (with  $-1$  replacing  $c_-, c_+$ );  $\alpha, \rho_0 = \text{constants} > 0$ . We find the convenient solution

$$A_z = [e(c_- - c_+)]^{-1} \ln(F_1^{1/\alpha_+} F_2^{1/\alpha_-}), \quad \varphi = [c_+ / e(c_+ - c_-)] \ln(F_1^{c_- / c_+ \alpha_+} F_2^{1/\alpha_-}),$$

$$\rho_{v+} = \rho_{0+} \exp(-\alpha_+ \Gamma_+) = \rho_{0+} F_1, \quad \rho_{v-} = \rho_{0-} \exp(-\alpha_- \Gamma_-) = \rho_{0-} F_2, \tag{2}$$

with

$$F_1 = \left( \frac{4}{\alpha_+ K_1^2} \right) \left| \frac{\partial g_1}{\partial \eta} \right|^2 [1 + |g_1|^2]^{-2}, \quad F_2 = \left( \frac{4}{\alpha_- K_2^2} \right) \left| \frac{\partial g_2}{\partial \eta} \right|^2 [1 + |g_2|^2]^{-2},$$

where  $g_1, g_2$  are arbitrary functions of the complex variable  $\eta = x + iy$  and

$$K_1^2 = -e^2 c_0^2 \rho_{0+} (c_+ - c_-) 2\pi / c_-,$$

$$K_2^2 = -c_- K_1^2 \rho_{0-} / \rho_{0+} c_+;$$

$c_- < 0$  if the gun is operated with a positive center electrode.<sup>3</sup> The conditions  $\Gamma_{\pm} > 0$  imply  $A_z > 0$ . The magnetic field lines in the  $xy$  plane,  $F_1 F_2^{\alpha_+ / \alpha_-} = \text{const}$  ( $\tau$  lines), are in general different from the equipotential lines  $\varphi = \text{const}$  [they become nearly coincident if  $c_+ \sim c_-$ ; this case is consistent with a negative center electrode; solutions other than (2) must be considered if  $c_+ = c_-$ ]. In the particular case  $F_1 = \text{const} F_2$  the two systems of lines are coincident and the net charge density is proportional to the mass density  $\rho$  (e.g., slightly positive plasma; some electrons are removed at the electrodes;  $\varphi \propto A_z$ ).  $g_1, g_2$  are chosen according to physical conditions on  $\rho$  and on the fields, in particular according to the periodicity of the filament arrangement

(e.g., a simple period  $2\pi/m$  on the  $y$  axis). Since ionization is high on CS and much smaller far from CS, we consider  $\rho_{\pm} \rightarrow 0$  for  $x \rightarrow \pm\infty$ , where practically only neutral atoms exist;  $B_x(x \rightarrow \pm\infty) \rightarrow 0$ ;  $B_y(x \rightarrow \pm\infty) \rightarrow B_{0\pm} = \text{const}$  ( $B_{0+} > B_{0-}$ ), etc. For convenience we can take  $g_1, g_2$  both of the same form  $g = a + (1+a^2)^{1/2} e^{m\eta}$  ( $a_1, a_2 = \text{const} > 0$ ) already used in a known treatment<sup>4</sup> of the plasma filaments (that treatment was confined to  $A_x = A_y = u_x = u_y = \rho_+ - \rho_- = 0$ ; ionization and recombination reactions were not considered). The explicit expressions for  $\psi(\varphi, A_z, \dots)$  in  $S$  define functions of  $\varphi, A_z, \dots$ , locally, with  $x, y$ , which play the role of the parameters, determining the connections between successive branches. The index  $\zeta$  corresponds to the local character of  $S_{\zeta}, \psi_{\zeta}$ ; by taking  $\psi_{\tau i} = v_{\tau} - D_{\tau i}^{1/2}$  (the pair of orthogonal components  $v_{\tau}, v_v$  replacing  $v_x, v_y$ ) for  $\mu_i \leq \mu_0$ , we have a particle flow collinear with the  $\tau$  lines in some  $(x, y)$  region. If  $C(\psi_{\tau i})^{-1/2}$  replaces  $C(\psi)$  in  $S = S_{\tau i}$ , the solution  $f = f_v + L(\mu_i) [C(\psi_{\tau i})^{-1/2}] C(D_{\tau i})$

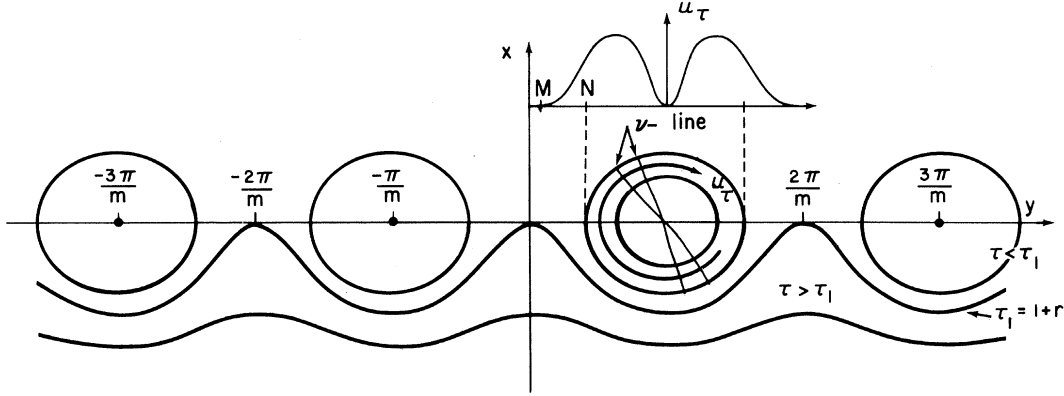


FIG. 2.  $E||v$ ;  $v \perp \tau$  lines.  $F \propto (\cosh mx + r \cos my)^{-2} = \tau^{-2}$ ;  $r = a(1+a^2)^{-1/2}$ .  $u_\tau$  (arbitrary scale) vs  $y$  is plotted in the upper diagram;  $u_\nu = 0$  inside all  $\tau_f(\mu_0)$  lines.

$\times f_\nu$  gives

$$\rho u_\tau \propto (\Gamma - \mu_i) L e^{-\alpha \mu_i} C(\mu_i - \Gamma).$$

With the spectrum  $L = e^{\alpha \mu_i} (b_0 + b_1 \mu_i + b_2 \mu_i^2) C(\mu_0 - \mu_i) d\mu_i$  in  $\int S_{\tau_i}$  we have  $\rho u_\tau = \gamma_0 [(\Gamma - \mu_{\min})(\Gamma - \mu_0)]^2 C(\mu_0 - \Gamma)$ ;  $b_0, b_1, b_2$  are defined as convenient polynomial combinations of  $\mu_0, \mu_{\min}, \gamma_0$ . Magnetic field lines and collinear flow on  $(x, y)$  are depicted in Fig. 2;  $\mu_{\min}, \mu_0$  are the values of  $\Gamma$ , respectively, on the filament axis (maximum of  $\rho$ ) and on some closed line  $\tau_f = \tau_f(\mu_0)$  crossing in the  $M$  the  $y$  axis (we have considered  $F_1 = F_2 = F, \rho_{0+} \geq \rho_{0-}$  and so  $\alpha_- \Gamma_- = \alpha_+ \Gamma_+ = -\ln F, \varphi \propto A_z$  for simplicity); the expression of  $\gamma_0$  in terms of the maximum value  $(\rho u_\tau)_{\max}$  of  $\rho u_\tau$  in the filament region is  $\gamma_0 = (\rho u_\tau)_{\max} (2/\Delta)^4, \Delta = \mu_0 - \mu_{\min}$ .  $N$  is given by the  $\tau$  line which best fits the visible-light profile of the filament; both  $M$  and  $N$  may coincide eventually at  $y = 0$  (see Fig. 2), then CS shows no filamentary structure by visible light but appears as a continuum (this is the case if the peak current  $I_{\max}$  across CA is increased to sufficiently high values<sup>5</sup>). The implication here is also that in this case a filamentary structure could be detected by other means than a visible-light photograph, e.g., by the associated gradients of electron density (schlieren images of a filamentary structure of CS have been observed<sup>6</sup>). The filamentary structure of CS for a CA with  $I_{\max} \sim 500$  kA (and 13 kV) is shown in Fig. 3. For  $\tau \geq \tau_f$  [e.g.,  $\tau \geq 1 + r$ , i.e., outside the filament region  $(x, y)$ ] we have  $|\vec{u}| = u_x$  if  $\psi = \psi_{xj}(\mu_j \geq \mu_0)$ ; a convenient spectrum  $L = C(\mu_j - \mu_0) e^{-\beta \mu_j} \sum_k d_k \mu_j^k, \beta > 0$ , gives  $u_x = 0$  on  $\tau_f, u_x \rightarrow \text{const} > 0$  for  $x \rightarrow -\infty$ , and  $j_x = 0$ , etc. From  $j_\tau$  we can estimate  $B_z$  (maximum value  $|B_{z0}|$  on the filament axis) if the values of the parameters  $\gamma_0, \mu_0, m$ , and  $r$  are introduced

from the experiments; in terms of the (absolute) maximum  $\rho_{\max}$  and (relative) minimum  $\rho_{\min}$  of  $\rho$ , on the  $y$  axis, we have  $r = (\rho_{\max}^{1/2} - \rho_{\min}^{1/2}) / (\rho_{\max}^{1/2} + \rho_{\min}^{1/2})$ . The magnitude of  $B_{z0} \cong 4\pi \times \int_0^x j_\tau(x, \tilde{y}) dx$ , where  $\tilde{y} = (2l+1)\pi/m, l = \text{integer}$ , and  $x_0 = \cosh^{-1}(\tau_f + r)/m$ , can be easily obtained by using the Laplace method ( $\Delta^{-1}$  is large if  $M$  is close to the filament axis). We have

$$B_{z0} \cong \pm e (\rho u_\tau)_{\max} 2\pi^{3/2} \Delta (\partial \Gamma / \partial x)_{x=\tilde{x}, y=\tilde{y}}^{-1},$$

if  $u_{\tau+} \gg u_{\tau-}$ ;  $\tilde{x}$  is given by  $\Gamma(\tilde{x}, \tilde{y}) = \frac{1}{2}(\mu_0 + \mu_{\min})$ . By taking  $\Delta / (\partial \Gamma / \partial x)_{\tilde{x}, \tilde{y}} \cong \ln[(1+r)/(1-r)] / (m \times \sinh m \tilde{x})$ ,  $\rho_{\max} / \rho_{\min} \sim 3, 2\pi/m \sim 2-4$  mm (see Fig. 3), and  $(\rho u_\tau)_{\max} \sim (10^{16} \text{ cm}^{-3}) u_0$ , one obtains values  $B_{z0} \sim 10^3-10^4$  G. We conclude that  $B_z$  inside the filaments can reach the same maximum values that the azimuthal component  $B_\theta \cong B_y$  takes in the down-stream region  $x > 0$ .  $B_z$  may have a different sign inside different filaments and is vanishing far from CS. Each filament is a bundle of helical magnetic field lines with a pitch

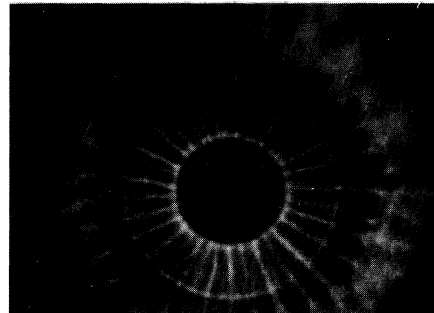


FIG. 3. Front view of CS rolling off the end of the center electrode. Image-converter photograph by visible light; 5-nsec exposure (at  $t = -120 \pm 20$  nsec; see text). The circular edge of the center electrode (diameter 3.4 cm) is visible in the background.  $D_2$  initial pressure 8 Torr.

increasing from the periphery to the axis of each filament. The ion orbits are definitely non-adiabatic on CS. A filament on the CS can perform as a "corkscrew" device<sup>7</sup> (Sinel'nikov magnetic trap) for particles reaching CS with a large velocity component  $v_z$ . A cyclotron resonant transfer of kinetic energy occurs from  $z$  direction (that we consider from now on as defined by the filament axis) into the Larmor rotation. We notice that the Larmor radius for ions with a velocity  $\lesssim u_0 \perp B_z \sim 2500$  G and the optical radius of a filament  $\sim 0.5$  mm (see Fig. 3) are of the same order of magnitude. At the dense focus stage, the CS is partially collapsed into a plasma column in the direction of the electrode axis; the filaments blend, optically, into a cylindrical pattern (the plasma column) starting from the end of the center electrode, but the filaments can still be observed individually in the off-axis, still advancing part of CS.<sup>8</sup> Time dependence, as well as  $z$  dependence, then becomes necessary. It is possible, however, to see from our static solutions that even a small rearrangement in mass flow or net charge distribution can produce drastic changes in  $\bar{j}$  and so large  $\partial \bar{B}/\partial t$  and large  $\bar{E}$  fields which can accelerate relatively few particles. The existence on CS of filamentary magnetic structures (with  $B^2/8\pi \sim$  kinetic-energy density<sup>9</sup>) is relevant for some unsettled points about the focus dynamics:

(A) When CS reaches the axis, the derivative of the CA current  $\partial I/\partial t$  shows a sharp minimum (commonly used as a time mark,  $t=0$ , for the events at the focus); the commencement of neutron production usually occurs at  $t \cong 0$ , but the main neutron pulse (after time-of-flight correction) reaches its maximum about 60 nsec (or more) later.<sup>8,10</sup> This indicates the existence of a delay  $\Delta t \geq 60$  nsec of the neutron maximum with respect to maximum compression on the column, which occurs near the center electrode at  $t=0$ .<sup>8</sup>

(B) The neutron pulse lasts  $t_n \sim 200$  nsec or more; the axial center-of-mass velocity of the reacting deuteron is  $u_d \cong 2 \times 10^8$  cm/sec<sup>11</sup>; neutron-generating plasma moving with a velocity  $\sim u_d$  would imply a plasma column length  $P \cong t_n u_d \sim 10$ -20 cm (this is a well-known contradiction with the laboratory observation  $P \sim 2.5$  cm).<sup>11</sup> The long-lasting neutron production can be easily associated with the relatively slow decay of the magnetic structure in the column. The  $B_z$  variations are responsible in part for the acceleration of reacting deuterons which collide predominantly in the radial direction<sup>11</sup>;  $B_\theta$  variations are

responsible for  $u_d$ . There is some evidence that the delay  $\Delta t$  of the neutron maximum corresponds to the relaxation time of the  $\bar{u}$ ,  $\rho$  rearrangements which trigger the field decay at some point of the column. As an example,  $|\nabla \rho_-|$  (by schlieren) disappears on the central column after the maximum compression but before the neutron maximum.<sup>12</sup>

We wish to thank W. H. Bostick, L. Grunberger, and W. Prior who obtained the photograph in Fig. 3.

---

\*Research sponsored in part by the U. S. Air Force Office of Scientific Research, Office of Aerospace Research, Grant No. AFOSR-70-1842.

<sup>1</sup>W. H. Bostick, L. Grunberger, V. Nardi, and W. Prior, in *Proceedings of the Ninth International Conference on Phenomena in Ionized Gases, Bucharest, 1969*, edited by G. Musa *et al.* (Institute of Physics, Bucharest, Romania, 1969), p. 66.

<sup>2</sup>W. H. Bostick, W. Prior, L. Grunberger, and G. Emmert, *Phys. Fluids* **9**, 2078 (1966).

<sup>3</sup>By algebraic transformations each of our Poisson equations is reduced to a pair of equations of the kind  $\partial^2 \Gamma / \partial \eta \partial \bar{\eta} = e^{\lambda \Gamma}$ ,  $\lambda = \text{const}$ ,  $\eta \bar{\eta} = |\eta|^2$ , which has a known integral. See C. Jordan, *Cours d'Analyse* (Gauthier Villars et Fils, Paris, 1896), Vol. 3, pp. 358-360. The given conditions on  $\rho_s$ ,  $\mathbf{j}_{es}$  (and the forthcoming constraints on  $u_x$ ,  $u_y$ ) can all be met by conveniently specifying  $L(\mu_i)$ .

<sup>4</sup>V. M. Fadeev, I. F. Kvartskhava, and N. N. Komarov, *Nucl. Fusion* **5**, 202 (1965).

<sup>5</sup>J. W. Mather and A. H. Williams, *Phys. Fluids* **9**, 2080 (1966).

<sup>6</sup>J. P. Baconnet, G. Cesari, A. Coudeville, and J. P. Watteau, in *Proceedings of the Ninth International Conference on Phenomena in Ionized Gases, Bucharest, 1969*, edited by G. Musa *et al.* (Institute of Physics, Bucharest, Romania, 1969), p. 665. Schlieren images of CS obtained by W. Bostick and W. Prior at Stevens Institute of Technology with the low  $D_2$  pressure  $\sim 0.6$  Torr show a filamentary structure even if the image-converter photographs (simultaneously taken) do not reveal any filament by visible light (private communication).

<sup>7</sup>H. Dreicer, H. J. Karr, E. A. Knapp, J. A. Phillips, E. J. Stovall, and J. L. Tuck, *Nucl. Fusion, Suppl.* No. 1, 299 (1962); K. D. Sinel'nikov, B. N. Rutkevich, and V. D. Fedorchenko, *Zh. Tekh. Fiz.* **30**, 249 (1960) [*Sov. Phys. Tech. Phys.* **5**, 229 (1960)].

<sup>8</sup>W. H. Bostick, L. Grunberger, and W. Prior, *Proceedings of the Third European Conference on Controlled Fusion and Plasma Physics, Utrecht, The Netherlands, 1969* (Wolters-Noordhoff Publishing, Groningen, The Netherlands, 1969), p. 120.

<sup>9</sup>The  $B_z$  contribution could be even smaller without impairing the argument that the reacting deuterons receive most of their energy from the field. This is

possible if the field energy is transferred only to a fraction of plasma particles, for instance to particles matching some resonance condition similar to the static-corkscrew conditions; complications are introduced by field self-consistency and time dependence at the focus.

<sup>10</sup>J. P. Baconnet, G. Cesari, A. Coudeville, and J. P.

Watteau, in *Proceedings of the Ninth International Conference on Phenomena in Ionized Gases, Bucharest, 1969*, edited by G. Musa *et al.* (Institute of Physics, Bucharest, Romania, 1969), p. 643; H. L. L. van Paassen, *Phys. Fluids* **12**, 2193 (1969).

<sup>12</sup>J. P. Baconnet, G. Cesari, A. Condeville, and J. P. Watteau, to be published.

## TEMPERATURE-DEPENDENT TILT ANGLE IN THE SMECTIC C PHASE OF A LIQUID CRYSTAL\*

T. R. Taylor, S. L. Arora, and J. L. Ferguson

*Liquid Crystal Institute, Kent State University, Kent, Ohio 44240*

(Received 25 May 1970)

Measurement of the tilt angle of the smectic *C* phase of terephthal-bis-(4-*n*-butylaniline) has been made using conoscopic observation and circularly polarized light. The new phenomenon of a smectic *C* phase with a temperature-dependent tilt angle is reported. Terephthal-bis-(4-*n*-butylaniline) has nematic, smectic *A*, smectic *C*, and smectic *B* liquid-crystalline phases. The tilt angle of smectic *C* changes from 0° at the smectic-*A*-smectic-*C* transition to approximately 26° at the smectic-*C*-smectic-*B* transition temperature.

The most commonly occurring smectic phases have been classified according to optical texture as smectic *A*, *C*, and *B* by Sackmann and Demus.<sup>1</sup> Smectic phases are considered to be layered and smectic *A* has a molecular arrangement such that the long molecular axis is perpendicular to the layers; smectic *C* has the molecular axis tilted with respect to the layer normal. Smectic *B* can have the molecular axis perpendicular or tilted and, in addition, has an order within the layers.

The optical properties of terephthal-bis-(4-*n*-butylaniline) (TBBA) are of special interest because it has nematic, smectic *A*, smectic *C*, and smectic *B* phases. TBBA was prepared by refluxing 4-*n*-butylaniline (2 mole) and terephthalaldehyde (1 mole) in absolute ethanol for 5-6 h. The product after isolation was recrystallized several times from alcohol until the transition temperatures remained constant. Analysis calculated for C<sub>28</sub>H<sub>32</sub>N<sub>2</sub> was N, 7.07; found, N, 7.15. The phase-transition temperatures are isotropic-nematic, 236.5°; nematic-smectic *A*, 199.6°; smectic *A*-smectic *C*, 172.5°; smectic *C*-smectic *B*, 144.1°; and smectic *B*-solid, 113.0°C. The absolute error in the temperatures is estimated to be less than ±1.0°C with a repeatability of ±0.2°C. A differential thermal analysis (du Pont DTA 900) is shown for heating and cooling in Fig. 1. From the thermogram it is apparent that the smectic *A*-smectic *C* (S<sub>A</sub>-S<sub>C</sub>) transition energy is very low compared with any of the other mesophase transition energies. The as-

signments of the phases were made by optical texture<sup>1</sup> using a polarizing microscope with a heated stage. Smectic *A* can exhibit the focal-conic texture in thick sections but generally orients normally spontaneously in sections less than 0.1 mm thickness. Smectic *C* exhibits the smectic schlieren texture<sup>1</sup> with thickness less than 0.1 mm and smectic *B* gives a mosaic texture.

In examining TBBA we found that the smectic *C* schlieren texture showed a striking change in the order of the birefringence as a function of temperature when observed with white light. In smectic *C* phases which we have reported,<sup>2</sup> we had not observed a temperature dependence of

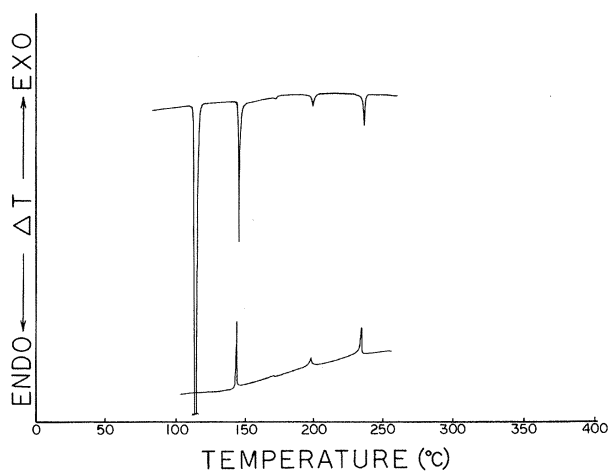


FIG. 1. Differential thermal analyzer thermogram of TBBA for heating and cooling.

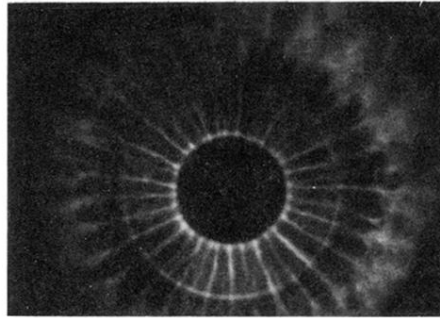


FIG. 3. Front view of CS rolling off the end of the center electrode. Image-converter photograph by visible light; 5-nsec exposure (at  $t = -120 \pm 20$  nsec; see text). The circular edge of the center electrode (diameter 3.4 cm) is visible in the background.  $D_2$  initial pressure 8 Torr.